Published in final edited form as:
Nanotechnology. 2014 January 10; 25(1): 014007. doi:10.1088/0957-4484/25/1/014007.

Using well-defined Ag nanocubes as substrates to quantify the spatial resolution and penetration depth of SERS imaging

Christine H Moran[1,2,4], **Matthew Rycenga**[1,4,5], **Xiaohu Xia**[1,2], **Claire M Cobley**[1], and **Younan Xia**[1,2,3]

Younan Xia: younan.xia@biomed.gatech.edu

[1]Department of Biomedical Engineering, Washington University, St. Louis, Missouri 63130, USA

[2]The Wallace H. Coulter Department of Biomedical Engineering, Georgia Institute of Technology and Emory University Medical School, Atlanta, Georgia 30332, United States

[3]School of Chemistry and Biochemistry, Georgia Institute of Technology, Atlanta, Georgia 30332, United States

Abstract

The multiplexing capability and high sensitivity of surface-enhanced Raman scattering (SERS) make this new imaging modality particularly attractive for rapid diagnosis. With 100-nm Ag nanocubes serving as the substrate, this work quantitatively evaluated, for the first time, some of the fundamental parameters of SERS imaging such as blur, spatial resolution, and penetration depth. Our results imply that SERS is a high-resolution imaging technique with a blur value of 0.5 μm that was lower than many traditional modalities such as mammography. The spatial resolution was measured to be 1.1 μm, suggesting that SERS images could be collected effectively by adjusting the imaging step size to the same length scale, or no more than 2 μm. The major drawback of SERS imaging is its penetration depth, which is limited by the scattering and absorption of tissues. We demonstrated that enhancement of signal caused by aggregation of multiple nanoparticles could help overcome this potential road-block to *in vivo* imaging.

Keywords

Surface-enhanced Raman scattering (SERS); imaging; silver nanocubes; optical imaging penetration depth

1. Introduction

Surface-enhanced Raman scattering (SERS) imaging recently emerged as an attractive modality owing to its multiplexing and fingerprinting capabilities, high sensitivity, and real-time data feedback [1–4]. The enhancement of Raman scattering signals from probe molecules on a noble-metal particle has allowed this modality to potentially compete with other optical imaging techniques based on fluorescence. When the localized surface plasmon resonance (LSPR) of Au or Ag nanoparticles functionalized with the probe molecules is excited by an incident light, the molecules will generate strong, unique signals *via* the SERS effect. By correlating the location of these signals with the peak intensity and wavenumber, SERS signals can be used to construct an image over small areas like a cell, or even larger areas like a tumor [1,5–11]. Essentially, SERS imaging takes advantage of the rich chemical

[4]These two authors contributed equally to this work.
[5]Present address: Department of Chemistry, Northwestern University, Evanston IL, USA

information contained in a typical SERS spectrum to generate images of nanoparticle distributions. Notably, the Raman spectrum of a molecule is like a human fingerprint – each type of molecule has a unique pattern. Therefore, by simply changing the molecules attached to the nanoparticle's surface, many distinctive SERS probes can be easily fabricated [3,4]. Moreover, since SERS bands are much narrower compared with fluorescent peaks, multiplexing of multiple probes, data analysis, and image reconstruction is easier and more accurate [1,3,4,9–11]. The narrow bands and unique nature of signals generated from different molecules allow for two or more different probes to be imaged simultaneously. Additionally, only a single excitation source is needed (unlike fluorescent molecules) to generate SERS from an array of different probe molecules.

The biomedical applications of SERS just began to be explored. The unique features of SERS as noted above make this technique ideal for developing specific detection assays and diagnostic tests [12]. Since the excitation source can be conveniently tuned to the near-infrared region (NIR) where soft tissue, blood, and water have minimum scattering and absorption, SERS has particular relevance to the field of *in vivo* detection and diagnosis.

In SERS imaging of biological samples, functionalized nanoparticles are usually conjugated with targeting ligands such as antibodies, peptides, or small molecules, achieving identification of cells and tissues with high specificity and affinity. Due to the multimodal properties of metal nanoparticles, SERS imaging can also be combined with other therapeutic and diagnostic applications [7,8]. For these reasons, SERS is an attractive imaging technique that may prove a useful tool, albeit for niche applications.

Despite these merits, the basic imaging parameters of SERS are rarely quantified. For example, the penetration depth of SERS is more or less limited when imaging biological samples due to the scattering and absorption by tissues, and thus deserves thorough investigation. In this work, the SERS images are closely compared with the corresponding physical objects – Ag nanocubes with a specific size, as well as well-defined separation and aggregation state. This allows us to be the first to characterize several important parameters of a SERS imaging system, including the blur and spatial resolution. In addition, phantoms are used to mimic some of the scattering and absorption properties of soft tissues in order to determine the effect of nanoparticle aggregation on the SERS signal intensity and thus penetration depth. By using phantom samples rather than animals, it was also much easier to identify the aggregation state of the nanoparticles and to quantitatively measure the penetration depth.

2. Materials and methods

2.1. Synthesis and functionalization of Ag nanocubes

The 100-nm Ag nanocubes were synthesized using a seed-mediated approach, and the detailed protocol can be found in our previous publication [13]. In brief, single-crystal, 30-nm Ag spherical seeds were prepared by reducing CF_3COOAg (Aldrich) to elemental Ag in ethylene glycol (EG, J. T. Baker). The seeds then grew in the presence of $AgNO_3$ (Aldrich) as a Ag precursor and poly(vinyl pyrrolidone) (PVP, $M_W \approx 55{,}000$, Aldrich) as a capping agent for the Ag{100} facets. When the major LSPR peak reached 585 nm as measured by a UV-vis spectrometer (Varian, Cary 50), the Ag nanocubes would have reached an edge length of 100 nm [14]. The reaction was immediately quenched using an ice-water bath and the resulting Ag nanocubes were washed once with acetone, and then thrice with deionized (DI) water to remove excess reactants. The final product was suspended in ethanol at a concentration of 10^{10}–10^{11} particles/mL for further use.

The Ag seeds and 100-nm Ag nanocubes were fully characterized by a UV-vis spectrometer, a scanning electron microscope (SEM, FEI, Nova NanoSEM 2300) operated at an accelerating voltage of 15 kV, and a transmission electron microscope (TEM, FEI, G2 Spirit) operated at 120 kV.

Functionalization of the Ag nanocubes was performed by mixing 10 μL of the as-prepared suspension to 100 μL of 1 mM 1,4-benzenedithiol (1,4-BDT, Aldrich) in ethanol. After incubation at room temperature for 1 h, the 1,4-BDT should have formed a self-assembled monolayer on the surface of the Ag nanocubes and could then be used as a SERS probe with well characterized SERS peaks [15].

2.2. Surface-enhanced Raman scattering

The SERS spectra were recorded using a Renishaw inVia confocal Raman spectrometer coupled with a Leica microscope with a 50× objective (NA = 0.9) in a backscattering configuration. The excitation wavelength used was 785 nm generated by a semiconductor c.w. diode laser equipped with a holographic notch filter based on a grating of 1200 lines/mm. Backscattered Raman signals were collected on a thermoelectrically cooled (−60 °C) CCD detector. The power of the laser was 3.1 mW, and the acquisition times varied, as noted, from 2–45 s.

Mapping was accomplished with a high-speed encoded stage (HSES) system capable of step sizes of 100 nm in the *x*, *y*, and *z* dimensions at speeds of 80 mm/s and a range of 112 mm in *x* and 76 mm in *y*. The two-dimensional SERS images were generated using Renishaw's WiRE Mapping Review software (Renishaw plc, Gloucestershire, UK). The peak at 1562 cm^{-1} for each data collection point was mapped as two-dimensional images based on the (*x*, *y*) coordinates, which provided a map of the spatial distributions of Ag nanocubes. The images were further modified with the WiRE software, or converted into a matrix with Origin software for the determination of peak-to-peak areas.

2.3. Determination of blur and resolution

We recorded SERS images from individual Ag nanocubes using the Renishaw Raman spectrometer. The samples were prepared by drop casting an ethanol suspension of the functionalized Ag nanocubes onto a Si substrate that had been patterned with registration marks *via* lithography or by simply scoring the substrate with a diamond pen. The substrate was briefly rinsed with ethanol to remove any dust that may interfere with locating the Ag nanocubes under a dark-field optical microscope. The Ag nanocubes were allowed to dry under ambient conditions and the locations of many nanocubes (typically 20 to 50) were identified by their Rayleigh scattering image using the dark-field microscope and their positions were noted for correlation with SEM. After the Ag nanocubes had been probed with SERS, the sample was immediately imaged by SEM to determine the sizes, shapes, and orientations of the nanocubes.

The SEM images, dark-field images, and two-dimensional SERS images were compared to determine the blur value of the SERS imaging system by measuring the diameter of the Ag nanocubes represented in each imaging modality. Resolution was calculated based on the ability to distinguish between two neighboring Ag nanocubes using a peak-to-peak area calculation. The signal intensity of the peak at 1562 cm^{-1} was plotted with respect to distance in the x-direction. As the area between the signal peaks of two neighboring Ag nanocubes approached zero, the resolution limit of the imaging system would be reached. The effect of imaging parameters on resolution was examined by collecting two-dimensional scans of functionalized Ag nanocubes on a Si substrate at different step sizes: 300 nm, 700

nm, 1.5 μm, 3 μm, and 5 μm. The SERS signals at different points were mapped, and the area between the peaks was calculated.

2.4. Calculation of point spread function

The lateral point spread function (PSF) of the confocal Raman microscope was plotted in Matlab v. 7.10 (Mathworks, Inc,. Natick, MA) using the following equation [16]:

$$\mathrm{PSF}(v)=\left|\frac{2J_1(v)}{v}\right|^4, \quad (1)$$

where J_1 is a first-order Bessel function of the first kind and *v* is the radial normalized optical coordinate:

$$v=\frac{2\pi\sin\gamma}{\lambda}r. \quad (2)$$

The radius, *r*, is the distance from the object point in the *x*, *y* plane, λ is the wavelength of the laser, and γ is the angle that defines the numerical aperture (NA) of the objective along with the refractive index, *n*, of the medium. This was calculated based on the following equation, with the NA of our system being 0.9:

$$0.9=n\sin\gamma. \quad (3)$$

2.5. Determination of penetration depth

The poly(vinyl alcohol) (PVA) gels were formed by allowing aqueous solutions of PVA to stand at room temperature. The mechanical properties were enhanced by freezing and then thawing the gel to encourage more cross-linking between the chains. This method is based on the concept of physical cross-linking, and avoids the need for additives or complex procedures involved in chemical cross-linking. By optimizing the number of freezing and thawing cycles, PVA gels with optical properties similar to those of soft tissue can be obtained [17]. Gels were cast and then frozen for 12 h followed by a thawing period of 12 h in one cycle, and 4 cycles were used to obtain the PVA phantoms used here. The SERS spectra were collected through the gel phantom from individual Ag nanocubes and aggregates of various sizes, as determined by the Rayleigh scattering image and SEM.

Chicken tissue was used to examine the impact of scattering in a realistic tissue environment. Chicken breast tissue, obtained from a local grocery store, was frozen and then sliced with a Xacto knife to obtain wedge-shaped pieces, such that the thickness increased gradually across its width. The tissue was placed on top of a monolayer of the functionalized Ag nanocubes. After focusing the laser on the surface of the Si coated with Ag nanocubes, SERS spectra were collected at 100 μm intervals through the tissue with increasing thickness. Signal intensity from the 1,4-BDT ring stretching mode at 1562 cm^{-1} was plotted at each point alongside the thickness of the tissue at that point. Processing of the raw SERS data was carried out using OriginPro v. 9, student version (OriginLab, Corp., Northampton, MA) and analysis was performed using Matlab.

3. Results and discussion

3.1. The blur and spatial resolution of SERS imaging

To determine the spatial resolution of our Raman system, we first characterized the blur value (B_v) associated with a SERS image. Blur takes into account the fact that an image is a

visual representation of a specific physical object [18]. Ideally, a small point within the object would be represented by a congruent point within the image. In reality, the image of each point in the object is blurred in the image, and can be modelled by the point spread function (PSF). The degree of blurring is quantified by B_v, the dimension of the image of a very small point object. Figure 1 shows the SEM image of a single nanocube with an edge length of 100 nm, as well as the Rayleigh scattering image and the SERS image of the same nanocube. The nanocube is small enough to be used as a point object from which B_v can be determined from the images. Values of 1.2 μm and 0.5 μm were determined for the B_v of Rayleigh scattering and SERS images, respectively. In contrast, typical blur values are 150 μm for mammography and 500 μm for photoacoustic tomography [18,19]. Figure 1(d) shows a plot of the lateral PSF as a function of the radial distance from the point object for our Raman imaging system. For imaging in air, as was the case in figure 1(a–c), the measured B_v correlates to the calculated full-width half-maximum (FWHM) of the PSF, which was 0.32 μm. This value is slightly better than the approximated B_v for SERS images taken in tissue and water, which were 0.44 and 0.42 μm, respectively.

Closely related to blur is spatial resolution, which describes the ability of an imaging system to distinguish objects that are close to each other. The ability of our Raman system to resolve individual nanoparticles that were closely spaced was determined to obtain the spatial resolution of the system. The spatial resolution of a particular imaging system can be inferred by the degree of blur, and is typically defined as the FWHM of the PSF [16,18]. From the above measurements of blur for a single nanocube we would expect to resolve nanocubes that are ~0.5 μm apart. To verify this, we designed an experiment where a linear array of nanocubes with different distances from one to another was formed on a Si substrate. Drop-casting a dilute suspension of nanocubes so that the outer edge of the meniscus slowly dried could yield such a linear array of nanocubes. Figure 2(a) shows the SEM image of an array of five nanocubes and figure 2(b) shows the Rayleigh scattering image from the same array. The red line in figure 2(b) shows the path of the Raman microprobe acquisition, and the peak intensity of the 1562 cm^{-1} band from 1,4-BDT was plotted along this line in figure 2(c). This graph shows that nanocubes with more than 2 μm separation from each other can easily be resolved in the SERS image with the naked eye. However, the resolution could be more precisely calculated by determining the area between the peaks, which has a correlation with the separation between the nanoparticles. As the area between the peaks (P_a) approached zero, the separation between the nanoparticles approached 1.1 μm, which represented the actual spatial resolution of our Raman system. This value was slightly greater than the resolution predicted by the PSF and blur value. This result suggests that Ag nanocubes with a separation less than 1.1 μm would appear as one object in the SERS image.

We also examined the effect of increasing the acquisition step size on the spatial resolution. A larger step size will decrease the number of acquisitions over an area and also reduce the acquisition time. In figure 3, a 9.6 × 9.3 μm^2 area was mapped with step sizes of 0.3 μm, 0.7 μm, 1.5 μm, 3 μm, and 5 μm, respectively. As the step size increased from 0.3 to 2 μm the resolution did not change dramatically. However, when the step-size increased beyond 2 μm, the resolution decreased, intensities decreased, and the individual nanocubes could no longer be identified in the SERS image. In addition, we measured P_a as a function of step size, as shown in figure 3h, which also shows a sharp decline in resolution beyond 2 μm. Since the spatial resolution of the Raman imaging system was determined to be 1.1 μm, using a step size smaller than the resolution will not make any difference in the resolution of the image but will needlessly increase the acquisition time.

3.2. Penetration depth of the SERS imaging system

3.2.1. Tissue penetration depth—Because SERS is an optical imaging method, it will be greatly influenced by tissue scattering and blood absorption [20,21]. The penetration depth is an important parameter which describes how deep light can travel into a material. For optical imaging this typically also includes the maximum thickness of tissue through which the detected signal can return to the surface and still be used for image construction. Since the SERS imaging in this study was performed using a confocal microscopy set-up, the spatial resolution of the system should not be adversely affected within the transport mean free path (TMFP) of NIR photons, about 1.1 mm for muscle tissue and 0.6 mm for brain tissue [22]. Should the tissue thickness exceed the TMFP, scattering will become a hindrance and severely reduce the spatial resolution [22,23]. Determination of the penetration depth is shown in figure 4(a), where a slice of chicken tissue with gradually increasing thickness was placed on top of a film of Ag nanocubes. The SERS signal of 1,4-BDT decreased as the thickness of the tissue increased. The penetration depth appears to be around 600 μm for this system using muscle tissue, which is much less than the TMFP of 1.1 mm in muscle. Since the tissue phantom is devoid of blood, fat, and skin, it would likely decrease slightly in an *in vivo* model. This simple study highlights that penetration depth is a major limiting factor in the use of SERS probes for deep *in vivo* tissue imaging.

3.2.2. Impact of Ag nanocube aggregation on SERS signal—Special considerations need to be made when using SERS as an *in vivo* imaging technique. While this study has shown that the penetration depth was quite shallow, around 600 μm, there are a range of penetration depths as determined from other groups, from 5.5 mm up to 1–2 cm [7,11]. SERS imaging studies typically do not investigate the morphology or the aggregation state of the nanoparticles in their images [2,3,7,15], even though it is well-known that aggregation affects the SERS signals dramatically [24]. In figure 4(b–f), nanocubes were deposited on a Si substrate and a PVA-gel was placed on top of them during the SERS measurements. A PVA phantom was used because the nanocubes could be visualized (by their Rayleigh scattering) through the nearly transparent gel. Figure 4(b) shows a side view of a typical phantom where d_s is the distance from the top of the gel to the Si substrate. The SERS signals from nanocubes with different morphologies (a single nanocube, a dimer, and a trimer as seen in figure 4(c–e)) were recorded. Figure 4(f) compares the intensities of the 1562 cm^{-1} band from 1,4-BDT supported on Ag nanocubes in three different aggregation states for a d_s value of 1.5 mm. It is clear that the SERS signals were detectable for all the different states of aggregation, with the signals strongly increased for the dimers and trimers. The SERS signal through the phantom was shown to increase by ×5 from a single particle to a dimer and ×10 from a single particle to a trimer. This simple demonstration clearly shows the role that aggregation plays in SERS imaging and suggests many prior studies involving Au and Ag nanoparticles might have relied on the aggregation even though this effect was never explicitly explored or stated [1–8,25]. The ability to obtain SERS images *in vivo* from tissues away from the skin surface should be largely determined by the aggregation states of nanoparticles, and not necessarily the SERS activity of individual nanoparticles [7].

4. Conclusion

This work represents the first characterization of the imaging capabilities and limitations of a SERS imaging system by using well-defined nanoparticles as the substrate. With our Raman system, we could resolve individual Ag nanocubes that were separated by a distance of ~1.1 μm on a Si substrate. Raman mapping step sizes below 2 μm did not dramatically increase the resolution, and could serve as the upper limit for SERS imaging of nanoparticle distributions. Importantly, in phantom experiments, SERS signals were shown to increase with the formation of simple aggregates such as dimers and trimers. Larger aggregates could

be responsible for some of the unusual penetration depths reported in the literature in addition to the resonance effects of the dyes used as probe molecules [7,11], although further investigation into how aggregation would affect the penetration depth is ongoing. Our data shows that nanoparticle aggregation is an important variable for SERS imaging *in vivo*, and that a better control over the aggregation state of nanoparticles may lead to greater penetration depths. However, as an optical imaging modality, there will be a limit to the depth of penetration and quality of images collected *in vivo*. SERS may best serve the medical imaging community as an endoscopic or *ex vivo* imaging technique which minimize tissue scattering effects.

Acknowledgments

This work was supported in part by a grant from the NIH (R01 CA138527) and startup funds from Georgia Institute of Technology.

References

1. Zavaleta CL, Smith BR, Walton I, Doering W, Davis G, Shojaei B, Natan MJ, Gambhir SS. Proc. Natl. Acad. Sci. 2009; 106:13511–13516. [PubMed: 19666578]
2. Kho KW, Fu CY, Dinish US, Olivo M. J. Biophotonics. 2011; 4:667–684. [PubMed: 21922673]
3. Lutz BR, Dentinger CE, Nguyen LN, Sun L, Zhang J, Allen AN, Chan S, Knudsen BS. ACS Nano. 2008; 2:2306–2314. [PubMed: 19206397]
4. Chen Y, Moran CH, Tan Z, Wooten AL, O'Sullivan JA. J. Raman Spectrosc. 2013; 44:703–709.
5. Kim J-H, Kim J-S, Choi H, Lee S-M, Jun B-H, Yu K-N, Kuk E, Kim Y-K, Jeong DH, Cho M-H, Lee Y-S. Anal. Chem. 2006; 78:6967–6972. [PubMed: 17007522]
6. Sha MY, Xu H, Natan MJ, Cromer R. J. Am. Chem. Soc. 2008; 130:17214–17215. [PubMed: 19053187]
7. Qian X, Peng X-H, Ansari DO, Yin-Goen Q, Chen GZ, Shin DM, Yang L, Young AN, Wang MD, Nie S. Nat. Biotech. 2008; 26:83–90.
8. Lee S, Kim S, Choo J, Shin SY, Lee YH, Choi HY, Ha S, Kang K, Oh CH. Anal. Chem. 2007; 79:916–922. [PubMed: 17263316]
9. Jun B-H, Kim J-H, Park H, Kim J-S, Yu K-N, Lee S-M, Choi H, Kwak S-Y, Kim Y-K, Jeong D, Cho M-H, Lee Y-S. J. Comb. Chem. 2007; 9:237–244. [PubMed: 17298100]
10. Sun L, et al. Nano Lett. 2007; 7:351–356. [PubMed: 17298000]
11. Keren S, Zavaleta C, Cheng Z, de la Zerda A, Gheysens O, Gambhir SS. Proc. Natl. Acad. Sci. 2008; 105:5844–5849. [PubMed: 18378895]
12. Xie W, Schlüker S. Phys. Chem. Chem. Phys. 2013; 15:5329–5344. [PubMed: 23482970]
13. Zhang Q, Li W, Moran C, Zeng J, Chen J, Wen L-P, Xia Y. J. Am. Chem. Soc. 2010; 132:11372–11378. [PubMed: 20698704]
14. Xia X, Zeng J, Oetjen LK, Li Q, Xia Y. J. Am. Chem. Soc. 2012; 134:1793–1801. [PubMed: 22206387]
15. Joo SW, Han SW, Kim K. J Colloid Interface Sci. 2001; 240:391–399. [PubMed: 11482946]
16. Wang, LV.; Wu, H. Biomedical Optics: Principles and Imaging. Hoboken, NJ: John Wiley & Sons; 2007. p. 166-167.
17. Kharine A, Manohar S, Seeton R, Kolkman RGM, Bolt RA, Steenbergen W, de Mul FFM. Phys. Med. Bio. 2003; 48:357–370. [PubMed: 12608612]
18. Sprawls, P. Physical Principles of Medical Imaging. Madison, WI: Medical Physics Pub Corp; 1995. Blur, Resolution, and Visibility of Detail.
19. Xu M, Wang LV. Rev. Sci. Instrum. 2006; 77:041101.
20. Ntziachristos V, Bremer C, Weissleder R. Eur. Radiol. 2003; 13:195–208. [PubMed: 12541130]
21. Zhang HF, Maslov K, Stoica G, Wang LV. Nat. Biotech. 2006; 24:848–851.
22. Ntziachristos V. Nat. Methods. 2010; 7:603–614. [PubMed: 20676081]

23. Liu Y, Zhang C, Wang LV. J. Biomed. Opt. 2012; 17:126014. [PubMed: 23232794]
24. Camargo PHC, Li W, Au L, Rycenga M, Xia Y. J. Phys. Chem. 2009; 484:304–308.
25. Chon H, Lee S, Son SW, Oh CH, Choo J. Anal. Chem. 2009; 81:3029–3034. [PubMed: 19301845]

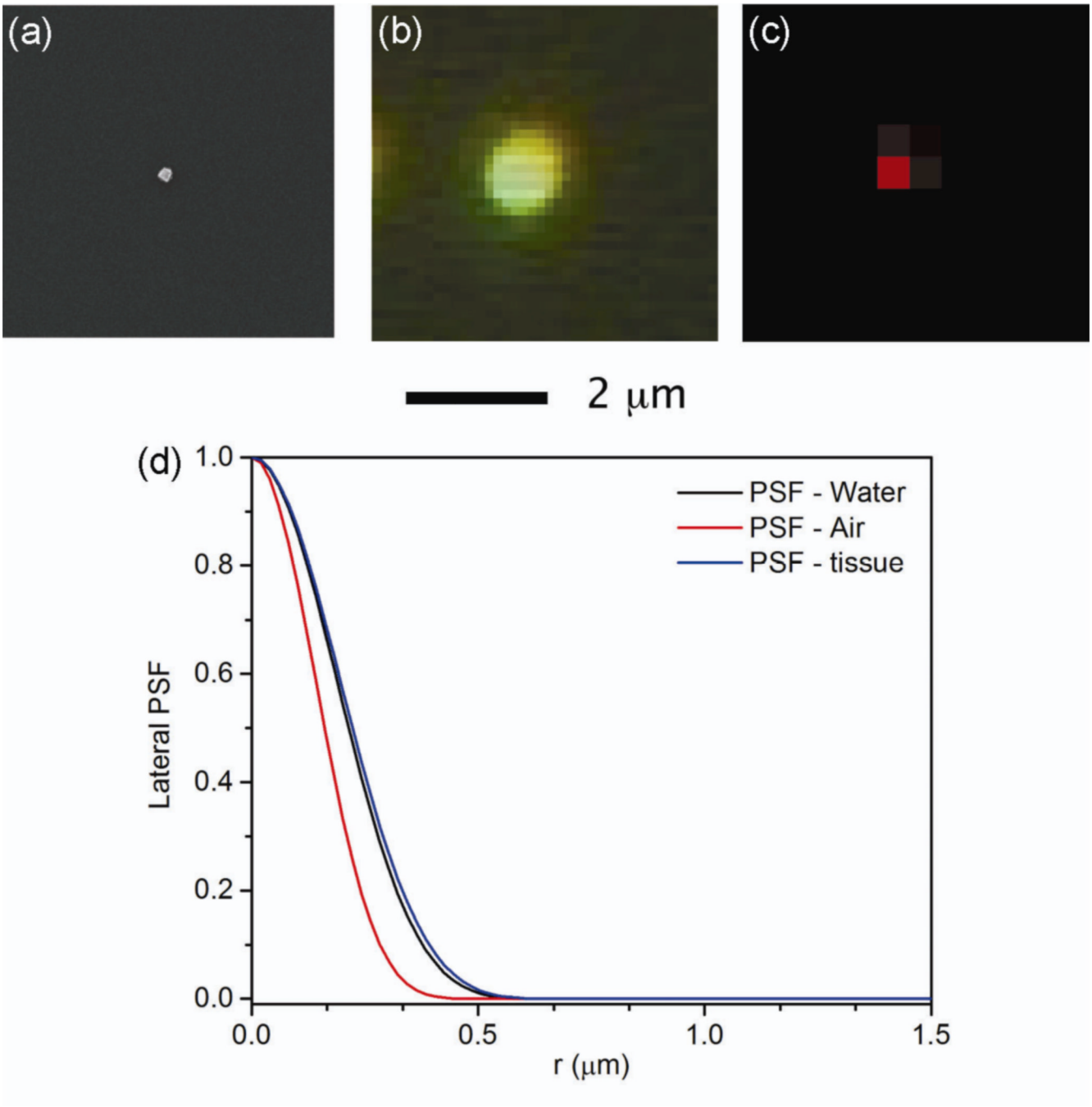

Figure 1.

The blur value (B_v) of our SERS imaging system was determined by measuring the diameter of the image of an individual Ag nanocube used as a point object. (a) SEM image of a Ag nanocube with an edge length of 100 nm that had functionalized with 1,4-BDT. (b) A dark-field image from the Rayleigh scattering of the same nanocube in (a). (c) SERS image of the same nanocube in (a). A B_v of 1.2 and 0.5 μm was measured for Rayleigh scattering and SERS imaging, respectively. (d) The measured blur values were compared to the calculated lateral point spread function (PSF) of our confocal Raman imaging system as a function of the radial distance from the object point. The FWHM in air was 0.32 μm, which was close to

the measured B_v of 0.5 μm of the SERS image. The PSF of the system in water and tissue were also calculated, and the B_v was found to increase slightly in these media to 0.42 μm and 0.44 μm respectively. λ_{ex} = 785 nm, t = 2 s, P = 3.1 mW.

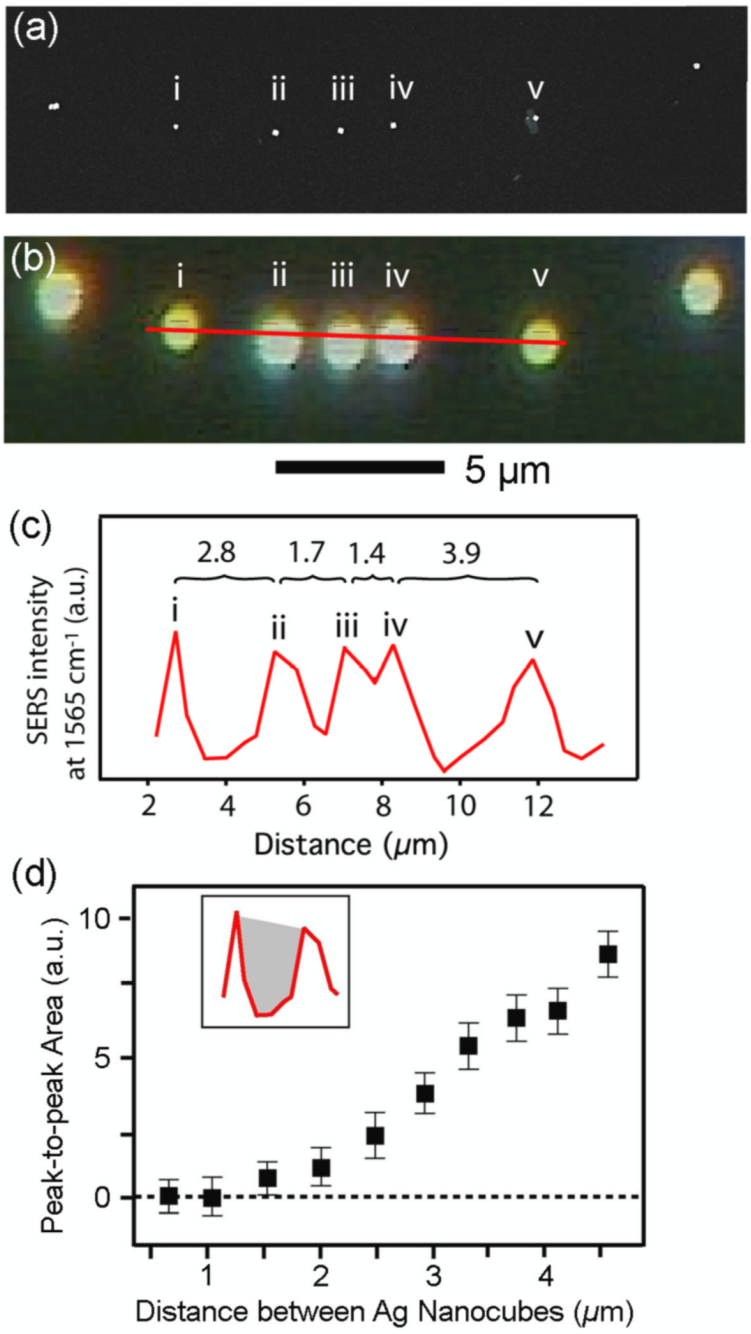

Figure 2.

(a) SEM image of Ag nanocubes (edge length: 100 nm, functionalized with 1,4-BDT) on a Si substrate and (b) the corresponding dark-field image. The red line represents the path of the Raman acquisition that included the five nanocubes labeled in (a). Data was acquired over this red line with a step size of 0.2 μm. The scale bar is 5 μm. (c) A plot of the SERS intensity at 1562 cm^{-1} along the red line shown in (b), which clearly resolves the nanocubes. The distance between (i) and (ii) was 2.8 μm; (ii) and (iii) was 1.7 μm; (iii) and (iv) was 1.4 μm; and (iv) and (v) was 3.9 μm. (d) The peak-to-peak area (P_a) is a tool to quantitatively determine the resolution. The area between the peaks in (c), shown in the insert as the gray shaded region, was plotted as a function of the distance between neighboring nanocubes. As

the distance between neighboring nanocubes approached 1.1 μm, P_a approaches 0, indicating that 1.1 μm is the spatial resolution. λ_{ex} = 785 nm, t = 2 s, P = 3.1 mW.

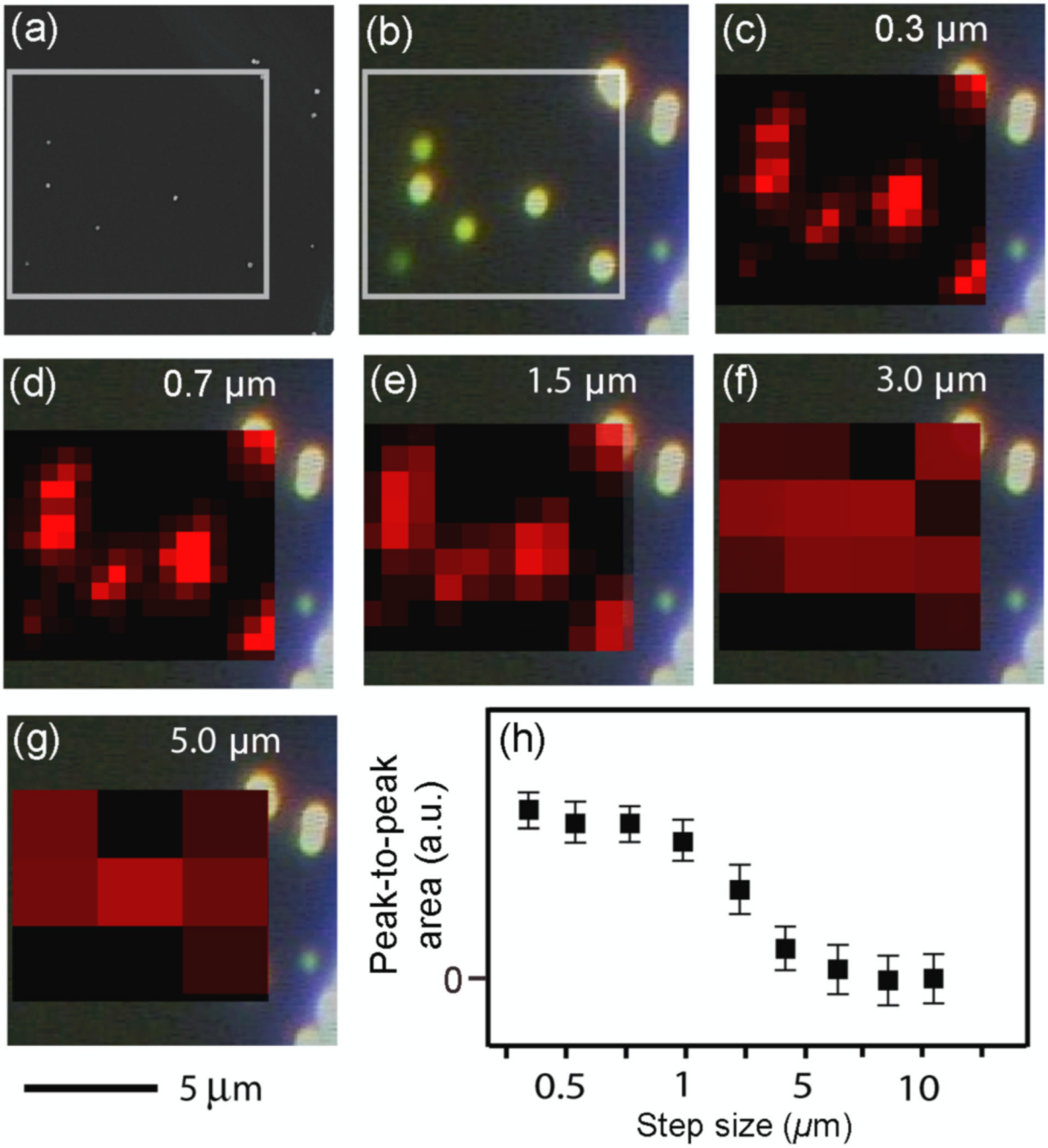

Figure 3.

(a) SEM image of 100-nm Ag nanocubes functionalized with 1,4-BDT with the white box corresponding to the SERS mapping area (9.6 × 9.3 μm^2). (b) The corresponding dark-field scattering image from (a). In (c–g) the SERS intensity of the 1562 cm^{-1} peak from the Ag nanocubes is mapped with different step sizes as indicated in the SERS map. λ_{ex} = 785 nm, t = 2 s, P = 3.1 mW. (h) A plot of the area between the SERS peaks for nanocubes (P_a) as a function of the acquisition step size, demonstrating that a step size smaller than the resolution of the system has little effect on the resolution, and that dramatically increasing the step size worsens the resolution. The 5 μm scale bar applies to images in (a)–(g).

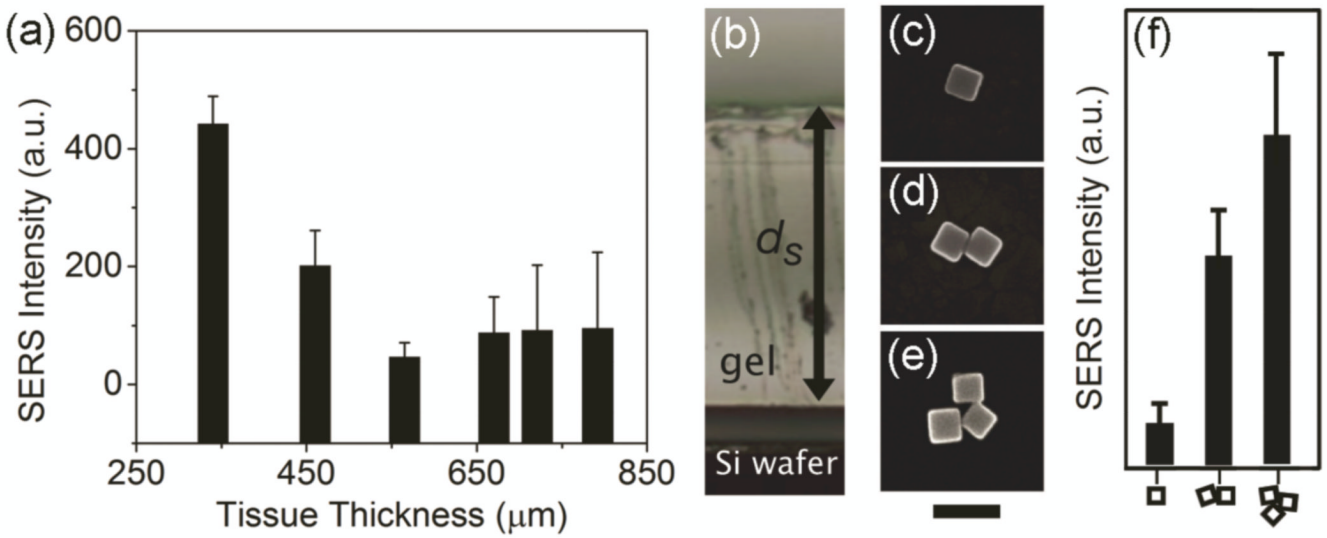

Figure 4.

(a) The SERS intensity of the 1562 cm^{-1} peak from 4-BDT functionalized nanocubes as a function of the thickness of chicken breast tissue measured at 100 μm intervals along a one-dimensional path. As the thickness of the tissue increases from 380 to 800 μm the SERS signal decreases and becomes non-detectable. λ_{ex} = 785 nm, t = 45 s, P = 3.1 mW (b) Image of a PVA-gel on top a Si substrate that supported nanocubes. The distance from the top of the gel and the Si substrate is labeled d_s. The SERS was recorded from single nanoparticles, dimers, and trimers with a d_s of 1.5 mm. (c–e) Typical SEM images of the nanocubes and their dimer and trimer configurations. Scale bar is 100 nm. (f) The relative SERS intensities from nanocubes with the morphologies indicated on the bottom axis. λ_{ex} = 785 nm, t = 5 s, P = 3.1 mW.